Journal of Fluids and Structures (2001) **15,** 489–501
doi:10.1006/jfls.2000.0350, available online at http://www.idealibrary.com on IDEAL®

MEAN AND FLUCTUATING VELOCITY FIELDS IN THE WAKE OF A FREELY-VIBRATING CYLINDER

R. Govardhan and C. H. K. Williamson

Sibley School of Mechanical and Aerospace Engineering, Upson Hall
Cornell University, Ithaca, NY 14853–7501, U.S.A.

(Received 7 September 2000, and in final form 7 November 2000)

In the present work, we study the wake velocity field of an elastically mounted rigid cylinder oscillating transverse to a fluid flow, using DPIV measurements. It is shown that there are large qualitative changes in these velocity fields, depending on the mode of cylinder oscillation. In particular, the characteristic "recirculation bubble", usually seen in the mean velocity field behind the nonoscillating cylinder, is found to be present in the case of the '2S' wake formation mode, yet is completely absent for the '2P' mode. For the '2P' mode, we find instead the appearance of a pair of counter-rotating vortices of opposite sign to what is expected, causing a downstream-oriented jet-type flow close to the cylinder, which in turn results in a 'double-wake' type velocity profile. Measurements of both the total Reynolds stresses, and the periodic stresses evaluated using phase-averaged velocity data, show that more than 90% of the total stresses are due to the repeatable large-scale coherent structures in the wake, when the body is vibrating. Periodic stresses make up only about 60% of the total stresses, in the case of the stationary body. Interestingly, for the fixed body, the periodic stresses remain relatively unchanged between our experiments ($Re = 3900$) and those of Cantwell & Coles, at $Re = 140\,000$, although the total stresses are significantly increased at the larger Re. Our experimental evaluation of Reynolds stress is stimulated by the need for such data in developing turbulence modelling of these flows, as well as to enable detailed comparison with direct numerical simulations.

1. INTRODUCTION

The problem of vortex-induced vibration of a cylinder, in particular the case where a rigid circular cylinder is elastically mounted and constrained to oscillate transversely to a free stream, has been well-studied in the literature, as may be seen from the comprehensive reviews of Sarpkaya (1979), Bearman (1984) and Parkinson (1989). However, apart from the early work of Griffin (1971) where selected wake velocity profiles were measured at low $Re \approx 200$, from forced transverse oscillations of the cylinder, there have been no detailed investigations of the mean and fluctuating wake velocity fields for such a transversely oscillating cylinder. It should be mentioned here that the motivation for the present study of the wake velocity field, over a range of Reynolds numbers, $Re = 3000–4000$, comes from Stansby & Apsley (2000) and from Peter Stansby, Julio Meneghini and Hugh Blackburn (private communications), who are using turbulence modelling to predict the behaviour of an elastically mounted cylinder at high Re, and for which detailed experimental measurements of the velocity field are useful to validate the modelling procedure.

The amplitude response ($A^* = A/D$ = amplitude/diameter) of such an elastically mounted cylinder shows two distinctly different types of behaviours, depending on whether one has a high or low combined mass-damping parameter ($m^*\zeta$), as shown in Khalak & Williamson (1999) and Govardhan & Williamson (2000). [The mass ratio, $m^* =$ (mass of

0889–9746/01/040489 + 13 $35.00/0

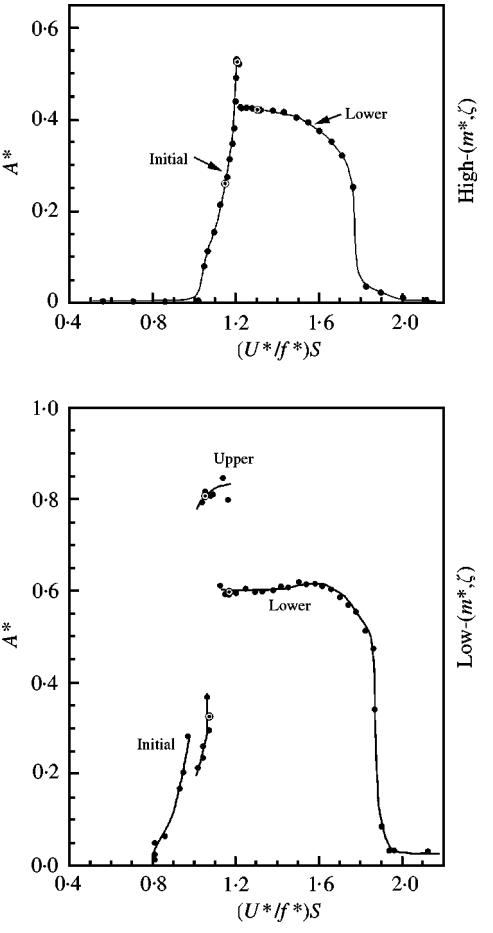

Figure 1. Amplitude response ($A^* = A/D$) of the elastically mounted cylinder as a function of flow speed. In the classical high-($m^*\zeta$) case, only 2 response branches ('Initial' & 'Lower') are seen, whereas in the low-($m^*\zeta$) case, a further higher amplitude 'Upper' branch of response is also observed. The flow speed parameter $(U^*/f^*)S = (f_{vo}/f)$, where f_{vo} is the stationary body shedding frequency, and f is the actual cylinder oscillation frequency. Mass-damping values for the two response plots shown are $(m^* + C_A)\zeta = 0{\cdot}251$ (High) and $(m^* + C_A)\zeta = 0{\cdot}013$ (Low), while the corresponding mass ratios are $m^* = 320$ and $m^* = 8{\cdot}63$, respectively. ●, Present response data; ⊙, location where the wake velocity field is measured.

oscillating structure)/(displaced mass of fluid); and the damping ratio ζ = structural damping/critical damping.] In the classical high-($m^*\zeta$) case, an 'Initial' and 'Lower' amplitude branch are separated by a discontinuous mode transition. However, in the case of low-($m^*\zeta$), a further higher amplitude 'Upper' branch of response appears, and there exist three response branches, as shown in Figure 1. There are therefore two mode transitions in this case. The existence of, not one, but two mode transitions at low-($m^*\zeta$), and their relationship with the forces and wake vortex dynamics, is studied in detail by simultaneous force, displacement and vorticity measurements for a freely vibrating cylinder in Govardhan & Williamson (2000). The present study of the wake velocity fields is related to work reported there.

Vorticity contours corresponding to the different response branches at low-($m^*\zeta$) shown in Figure 2, indicate that the Initial branch is associated with the 2S wake mode, while both

the Upper and Lower branches correspond to the 2P-mode; '2S' indicating 2 Single vortices formed per cycle, and '2P' meaning 2 Pairs of vortices formed per cycle, as defined by Williamson & Roshko (1988) based on their forced oscillation experiments. As may be seen from Figure 2, the strengths of the two vortices of each vortex pair are quite unequal in the Upper branch, but are roughly equal in the Lower branch. In the case of forced vibration, the 2S and 2P modes have also been shown using PIV by Carberry *et al.* (2001) for the forced transverse vibration of a circular cylinder, and these modes are also observed from forced oscillations of a tapered cylinder by Techet *et al.* (1998). At high values of the mass ratio, flow visualization of the wake of a freely vibrating wire also indicated a 2S and 2P mode, as shown by Brika & Laneville (1993).

In the present work, we study the mean and fluctuating velocity fields in the wake of a freely oscillating circular cylinder, at Re = 3000–4000, corresponding to each of the three response branches at low-$(m^*\zeta)$, namely the Initial, Upper and Lower branches. For comparison, a stationary cylinder case at approximately similar Reynolds numbers (Re = 3900) is also studied.

2. EXPERIMENTAL DETAILS

The present experiments were conducted using a hydroelastic facility, which is described in Khalak & Williamson (1999), in conjunction with the Cornell-ONR Water Channel. The hydroelastic facility comprises a carriage mounted on air-bearings situated above the channel test section, which allow a vertical cylinder in the fluid to move transverse to the free-stream. The turbulence level in the test section of the Water Channel was less than 0·9%, in the 0·381 m × 0·508 m cross section, over the range of free-stream velocities U (0·04–0·32 m s^{-1}) used in this study. The test cylinder had a diameter of 0·0381 m, and a length–diameter ratio of 10.

For the purpose of employing DPIV, the flow was seeded with 14 μm silver-coated glass spheres, which were illuminated by a sheet of laser light from a 5 W continuous Argon ion laser. Images of the particles were captured using a high-resolution CCD Kodak Megaplus (1008 × 1018 pixels) camera. Pairs of particle images were analysed using cross-correlation of sub-images, our implementation of which is described in more detail in Govardhan & Williamson (2000), and resulted in a set of 3600 vectors (60 × 60) for a typical velocity field. Each of the mean and fluctuating velocity fields shown in the paper have been obtained from about 300 such DPIV velocity fields.

The origin of the co-ordinate system is fixed at the centre of the cylinder, at zero flow speed. The x-axis is downstream, the y-axis is perpendicular to the flow direction and to the cylinder axis (defined as transverse), and the z-axis lies along the axis of the cylinder. The velocity components along the $\{x, y, z\}$ axes are denoted as $\{u, v, w\}$, respectively, and the freestream velocity is denoted as U. The Reynolds number, normalized velocity ($U^* = U/f_N D$), and oscillation amplitude ($A^* = A/D$) corresponding to each of the three cylinder response modes studied are: Initial (Re ≈ 3000, $U^* = 5{\cdot}18$, $A^* = 0{\cdot}33$); Upper (Re ≈ 3100, $U^* = 5{\cdot}33$, $A^* = 0{\cdot}81$); Lower (Re ≈ 3700, $U^* = 6{\cdot}40$, $A^* = 0{\cdot}60$).

3. MEAN VELOCITY FIELDS

Although the mean velocity field in the wake of a stationary cylinder has been extensively studied, relatively little is known about the velocity field in the wake of a transversely oscillating cylinder. The only detailed investigation of the velocity field (in the form of a set of velocity profiles) to our knowledge, was conducted by Griffin (1971), for the forced

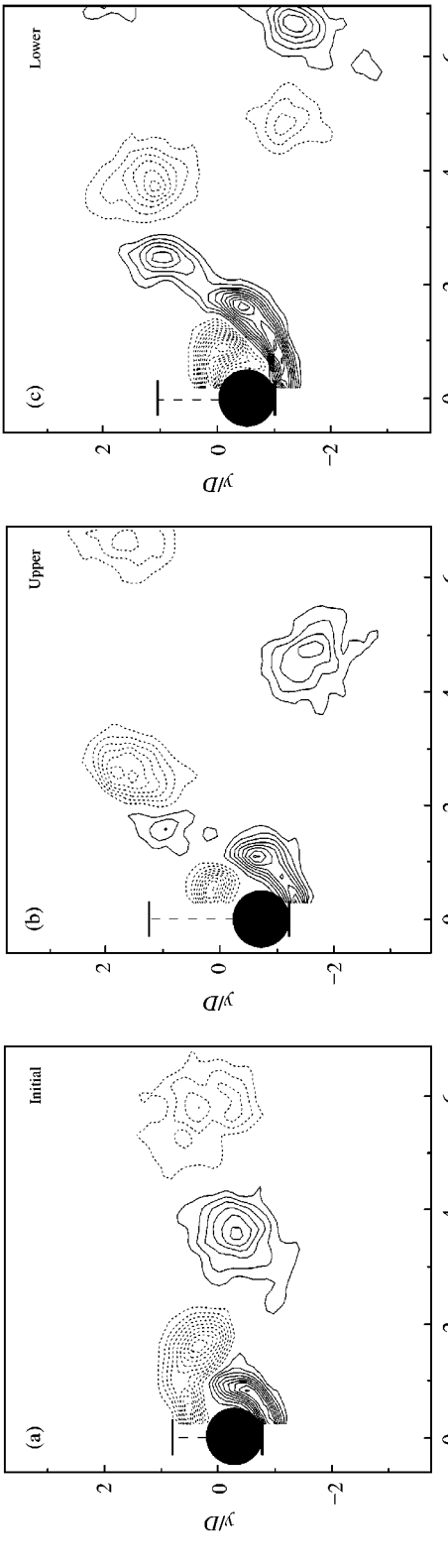

Figure 2. Vortex formation modes in the different response branches. (a) Initial branch - 2S; (b) Upper branch - 2P; (c) Lower branch - 2P. In the Upper branch case, there are two vortex pairs formed per cycle, although the second vortex of each pair is much weaker than the first vortex, and decays rapidly. The Initial, Upper, and Lower branch cases shown, in this and subsequent figures, correspond with data points marked as $\odot$ in the low-$(m^*\zeta)$ amplitude response plot in Figure 1. Vorticity contours levels shown are separated by $\Delta\omega D/U = 0{\cdot}4$. Solid contour lines denote anticlockwise vorticity and dashed lines are for clockwise vorticity. (a) Re $\approx$ 3000, $U^* = U/f_N D = 5{\cdot}18$, $A^* = 0{\cdot}33$; (b) Re $\approx$ 3100, $U^* = 5{\cdot}39$, $A^* = 0{\cdot}81$; (c) Re $\approx$ 3700, $U^* = 6{\cdot}40$, $A^* = 0{\cdot}60$.

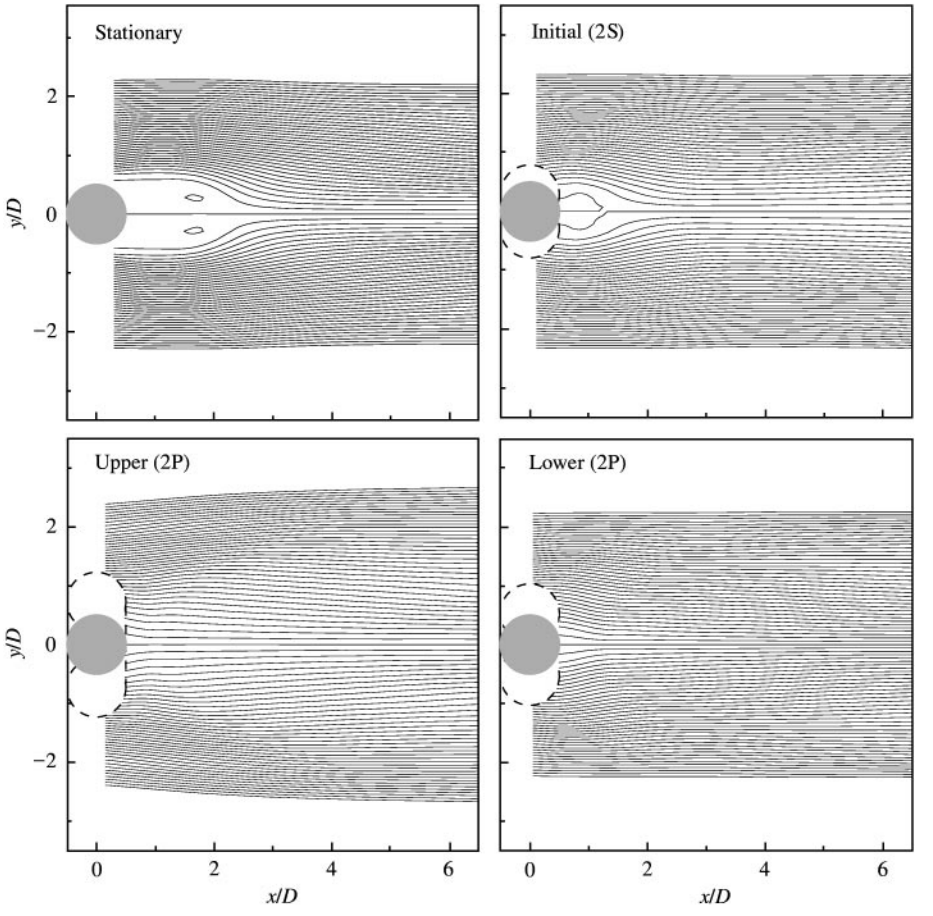

Figure 3. Streamlines for the mean velocity field indicating the disappearance of the "recirculation bubble" in the Upper and Lower branches which correspond to the 2P-mode. Re = 3900 for the stationary cylinder case shown here and in later figures.

vibration of a cylinder at low Re $\approx$ 200. He found that the formation length, defined as the location along the wake centreline where velocity fluctuations reach a maximum, reduced to half the value found for a stationary cylinder. It is expected that a similar reduction in size of the mean "recirculation bubble" will ensue when a body vibrates. At higher Re as in the present study (Re = 3000–4000), one might expect large deviations in the mean velocity field for the 2P-mode as compared with the wake of the 2S-mode, where the vortices are arranged as in a Kármán vortex street.

The streamlines for the mean velocity field corresponding to the Initial branch (2S-mode) in Figure 3, show the presence of a "recirculation bubble", as in the stationary cylinder case. The effect of body vibration, for the 2S-mode, is to markedly shorten the bubble, which is consistent with the reduced "formation length" for an oscillating body found by Griffin (1971). Interestingly, this "recirculation bubble" disappears for the Upper and Lower response branches that are associated with the 2P-mode, as may be seen in Figure 3.

The mean vorticity field, shown in Figure 4, for the Lower branch (2P-mode) shows the presence of a pair of counter-rotating vortices of opposite sign to what one might expect in a wake, in contrast to the Initial branch (2S-mode) case. The jet flow induced by this vortex

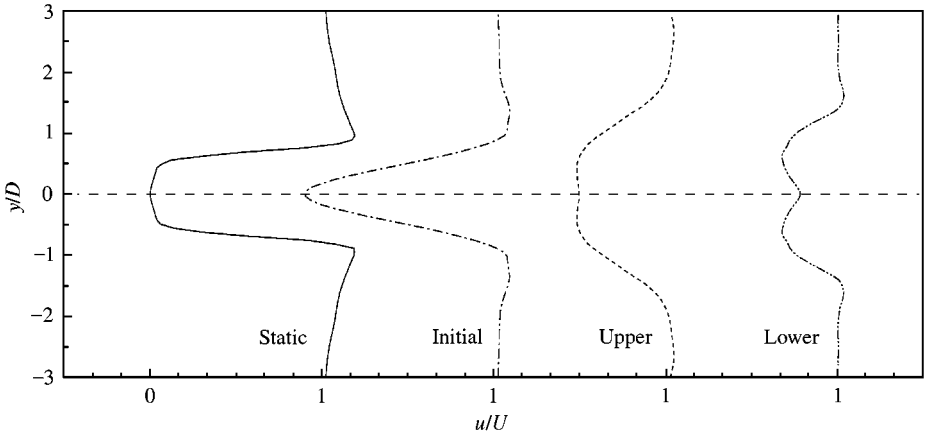

Figure 5. Streamwise velocity profiles at $x/D = 1{\cdot}25$. In the Lower branch (2P-mode), the velocity profile takes on the appearance of a 'double-wake' profile, due to the jet flow induced by the presence of counter-rotating vortices of opposite sign to what is expected in the wake.

pair, gives the streamwise mean velocity profile a 'double-wake' type appearance, as may be seen in Figure 5. It should be mentioned here that this type of 'double-wake' profile was observed by Koochesfahani (1989) for a mode of vortex formation downstream of a pitching airfoil, which is equivalent to the present 2P-mode. In the Upper branch (unequal 2P-mode) case, the mean vortex pair is again present in the mean vorticity field, although in this case it is rather weaker than for the Lower branch case, hence the 'double-wake' profile is only just discernible. The mean vortex pair, in the case of the 2P-modes found here, may be interpreted as due to vorticity being drawn across the wake, to form the second vortex in each pair of the 2P-mode. It has a sign of vorticity opposite to the classical wake vorticity. The detailed formation of the 2P-mode is described further in Govardhan & Williamson (2000).

4. FLUCTUATING VELOCITY FIELDS

We present, in this section, global mean Reynolds stresses in the wake, for the stationary cylinder as well as for the oscillating cylinder in each of the three branches of response, namely the Initial, Upper and Lower branches. In each case, the total Reynolds stress, computed from a large number of instantaneous DPIV velocity fields, as well as the periodic component of the Reynolds stress, calculated from phase-averaged velocity data as in Cantwell & Coles (1983), is shown. In the present work, the phase averaging of the velocity data is performed using the lift force signal as the reference, for the stationary cylinder, and using the cylinder displacement signal as a reference, for the oscillating cylinder cases. The set of instantaneous velocity fields obtained are divided into 30 different sub-groups, each sub-group corresponding to a certain phase of cylinder motion (or lift force), and the velocity fields within each sub-group are averaged. The periodic Reynolds stress is calculated from the resulting 30 phase-averaged velocity fields.

As discussed by Cantwell & Coles (1983), based on Reynolds & Hussain (1972), a flow variable $s(t)$ in the near wake can be viewed formally as a combination of a global mean component $\bar{s}$, a periodic mean component $\tilde{s}$ (which depends on the phase θ during a cycle), and a random component $s'(t)$. By definition, the total variable $s(t)$ is then the sum

$$s(t) = \bar{s} + \tilde{s}(\theta) + s'(t). \tag{1}$$

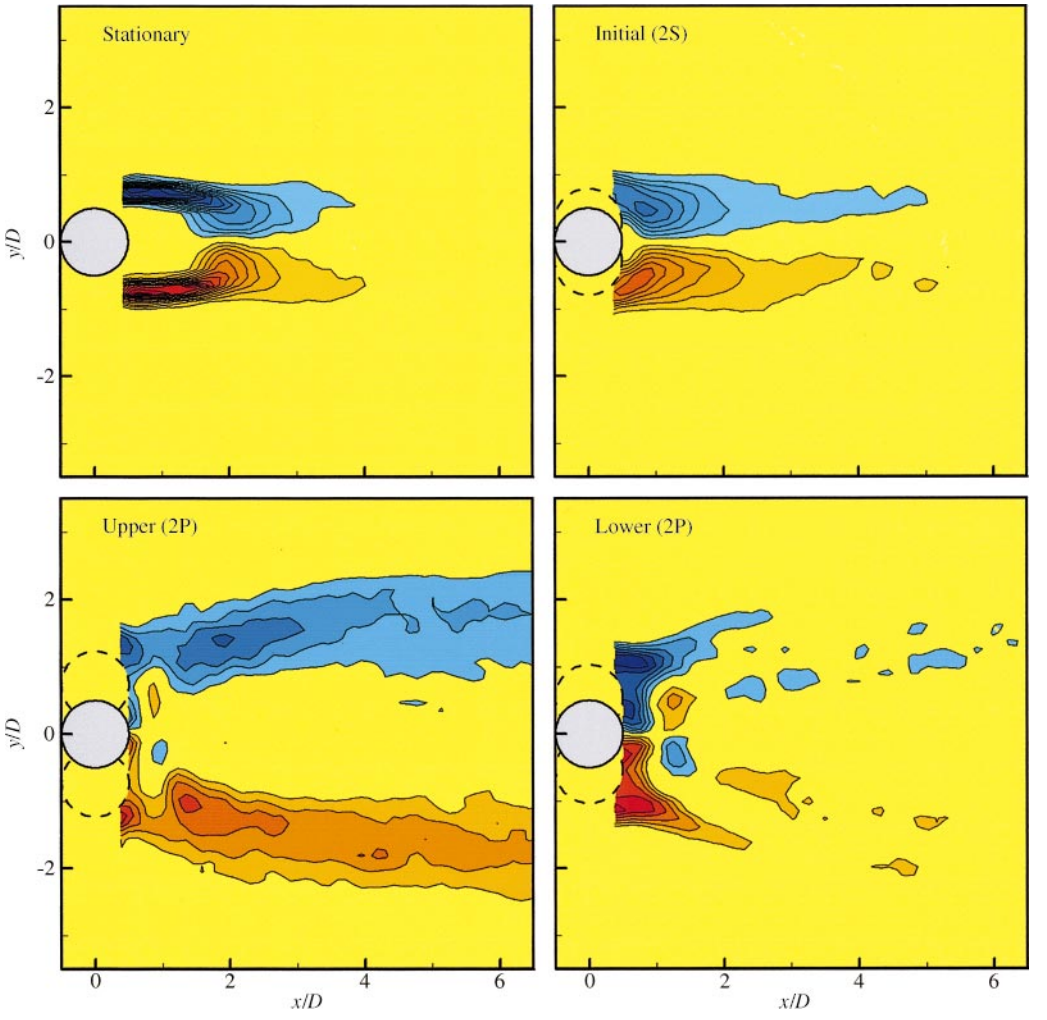

Figure 4. Mean vorticity fields showing the presence behind the cylinder of a pair of counter-rotating vortices of opposite sign to what is expected in a wake, for the Upper and Lower response branches, which correspond to the 2P-mode. Vorticity contours levels shown are $\omega D/U = \pm 0{\cdot}4$, $\pm 0{\cdot}8$, $\pm 1{\cdot}2 \ldots$ (for stationary cylinder and Initial branch), and $\omega D/U = \pm 0{\cdot}2$, $\pm 0{\cdot}4$, $\pm 0{\cdot}8 \ldots$ (for the Upper and Lower branches).

TABLE 1
Peak Reynolds stress in the wake of a stationary circular cylinder

(a) Total Reynolds stress		$(\overline{u''u''}/U^2)$	$(\overline{v''v''}/U^2)$	$(\overline{u''v''}/U^2)$
Cantwell & Coles (1983)	Re = 140 000	0·22	0·43	0·12
Present	Re = 3900	0·11	0·23	0·085
(b) Periodic part of Reynolds stress		$(\overline{\tilde{u}\tilde{u}}/U^2)$	$(\overline{\tilde{v}\tilde{v}}/U^2)$	$(\overline{\tilde{u}\tilde{v}}/U^2)$
Cantwell & Coles (1983)	Re = 140 000	0·08	0·23	0·05
Present	Re = 3900	0·065	0·18	0·06

The global mean $\bar{s}$, may be obtained by averaging over all the instantaneous velocity fields. On the other hand, in order to obtain the periodic mean $\tilde{s}(\theta)$, we need to average the data at constant phase of vortex shedding (θ), as in Cantwell & Coles (1983). Following the notation used in Cantwell & Coles (1983), the periodic component ($\tilde{s}$) may then be defined as

$$\tilde{s}(\theta) = \langle s \rangle_\theta - \bar{s}, \tag{2}$$

where $\langle s \rangle_\theta$ is the mean of s at a particular phase θ. In the present work, we also introduce the additional notation, $s''(t)$, as the total fluctuation, defined by

$$s''(t) = s(t) - \bar{s} = \tilde{s}(\theta) + s'(t). \tag{3}$$

If $s(t)$ is the streamwise velocity component $u(t)$, then the total streamwise Reynolds normal stress $(\overline{u''u''})$ would have two components; the periodic component $\overline{\tilde{u}\tilde{u}}$, due to the repeatable large-scale coherent structures in the wake, and the random component $\overline{u'u'}$, due to the random small-scale turbulence, as discussed in Cantwell & Coles (1983) and shown below:

$$\overline{u''u''} = \overline{\tilde{u}\tilde{u}} \qquad + \overline{u'u'}$$

$$\text{Total} = \text{Periodic} + \text{Random}$$

The peak value of the total streamwise Reynolds stress for the stationary cylinder, at our Re $\approx$ 3900, is about $(\overline{u''u''}/U^2) \approx 0{\cdot}11$, as may be seen from Figure 6. As one might expect, this value is substantially smaller than the peak value of $(\overline{u''u''}/U^2) \approx 0{\cdot}22$ found in the much higher Re (Re = 140 000) experiments of Cantwell & Coles (1983). However, if instead we now compare the peak periodic stress, we find interestingly that their values are quite similar, 0·065 and 0·08, respectively. In fact, comparison of the peak values of each of the other Reynolds stresses between the two widely different Reynolds numbers, also shown in Table 1, indicates that in each case, the peak periodic components are very nearly the same, although the peak total Reynolds stress is significantly larger for the higher Re experiments. This suggests that the repeatable large-scale coherent structures, responsible for the periodic part of the Reynolds stresses, are quite similar over the range of Re from 3900 to 140 000. Therefore, the increase in Reynolds stresses over this range of Re seems to be principally due to the random component. We suggest that this is fed by the increasing strength of the Kelvin–Helmholtz instability of the separating shear layer, as Re increases in this "Shear Layer instability regime", defined in the review of Williamson (1996), and first studied by Schiller & Linke (1933); see also Roshko's (1993) review.

For the stationary cylinder case, at our Re = 3900, the maximum total stress $(\overline{u''u''}/U^2)$ is about 0·11, while the periodic stress $(\overline{\tilde{u}\tilde{u}}/U^2) \approx 0{\cdot}065$, indicating that in this case the periodic

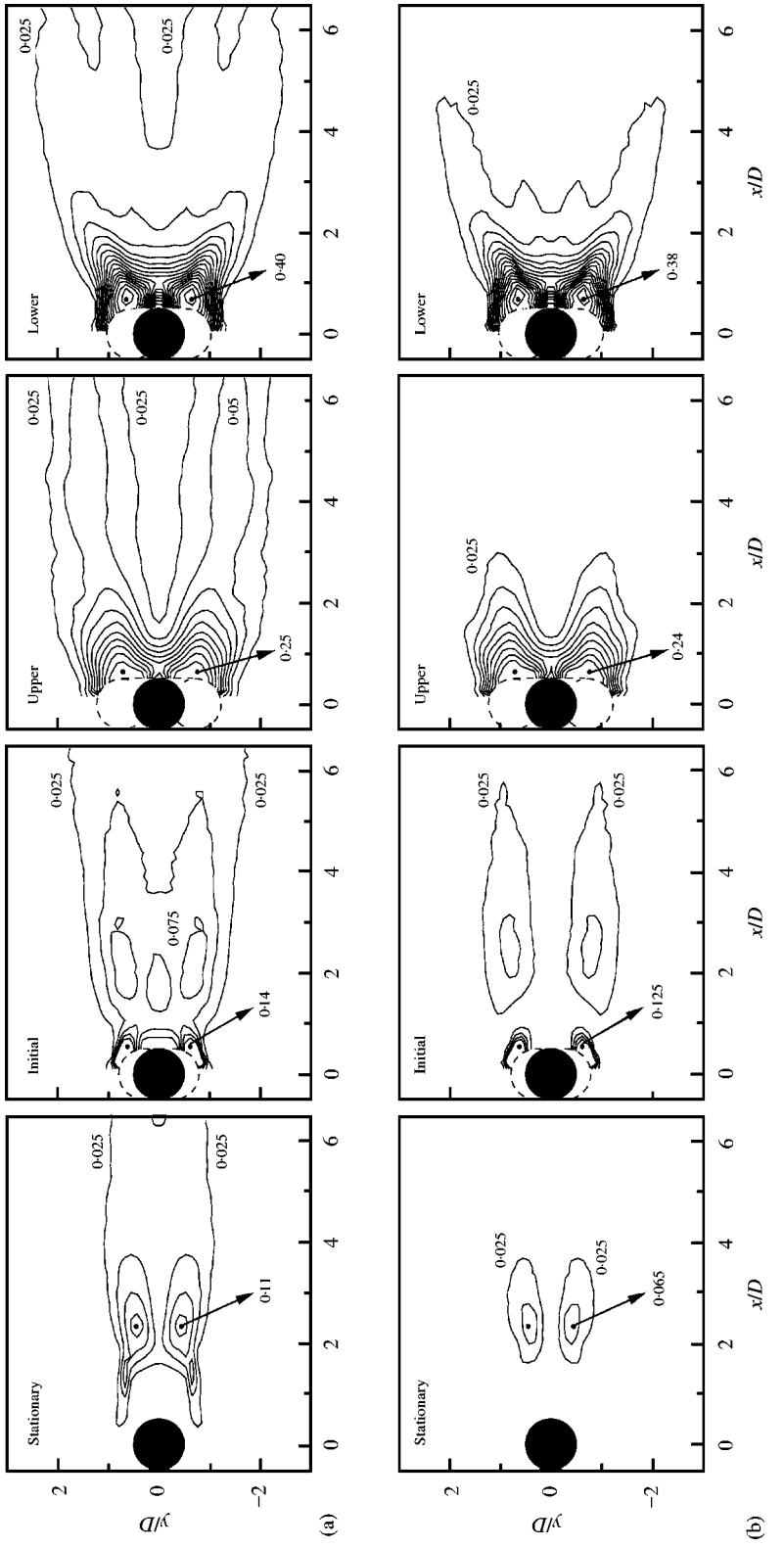

Figure 6. Contours of (a) total $(\overline{u''u''}/U^2)$ and (b) periodic component $(\overline{\tilde{u}\tilde{u}}/U^2)$ of the global mean streamwise Reynolds normal stress. The total Reynolds stress is calculated from a large number of instantaneous velocity fields, while the periodic part of the Reynolds stress is calculated from phase-averaged velocity data. Contours shown are separated by 0·025 for all cases. ●, location of the maximum value of the Reynolds stress.

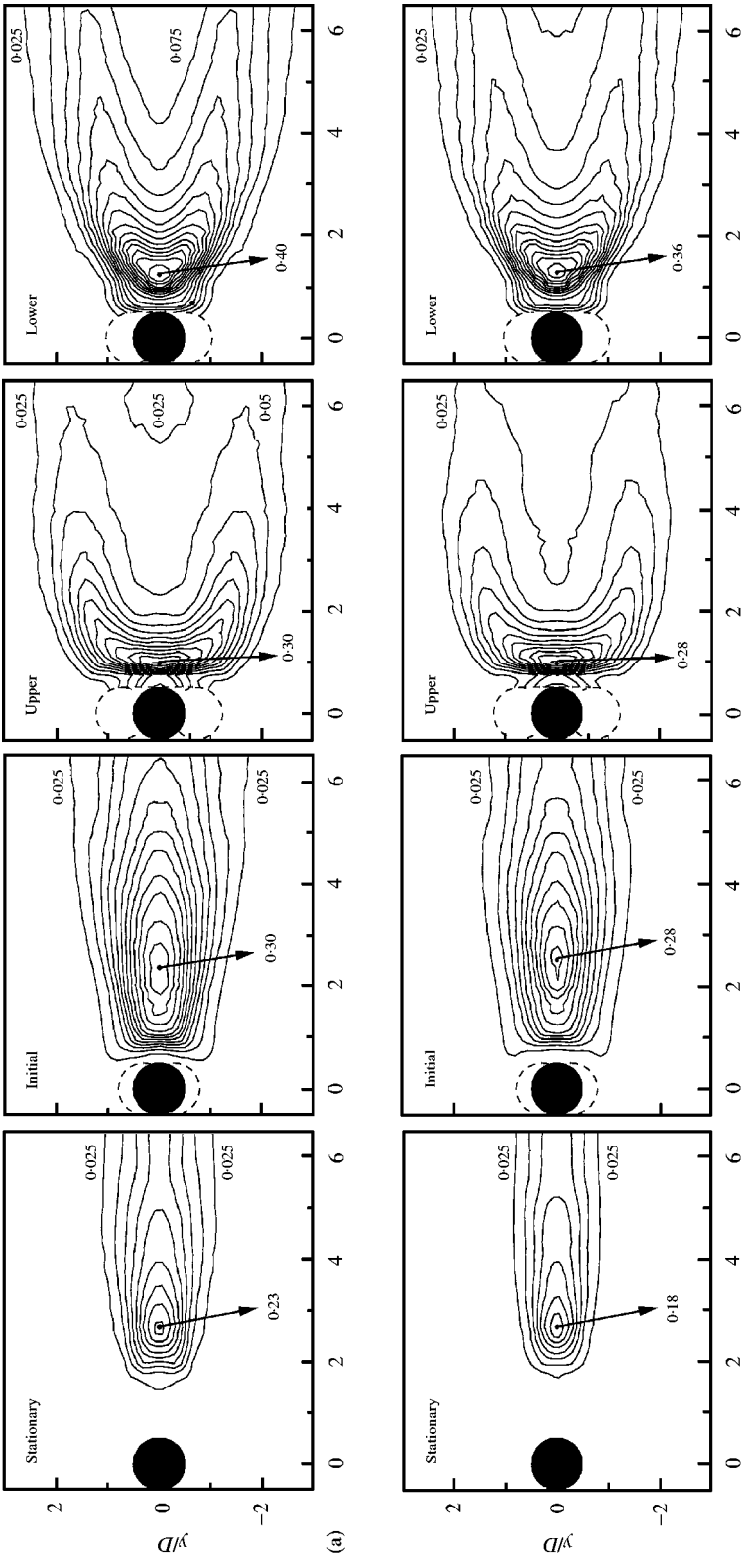

Figure 7. Contours of (a) total ($\overline{v''v''}/U^2$) and (b) periodic component ($\overline{\tilde{v}\tilde{v}}/U^2$) of the global mean crossflow Reynolds normal stress. Contours shown are separated by 0·025 for all the cases. ●, location of the maximum value of the Reynolds stress.

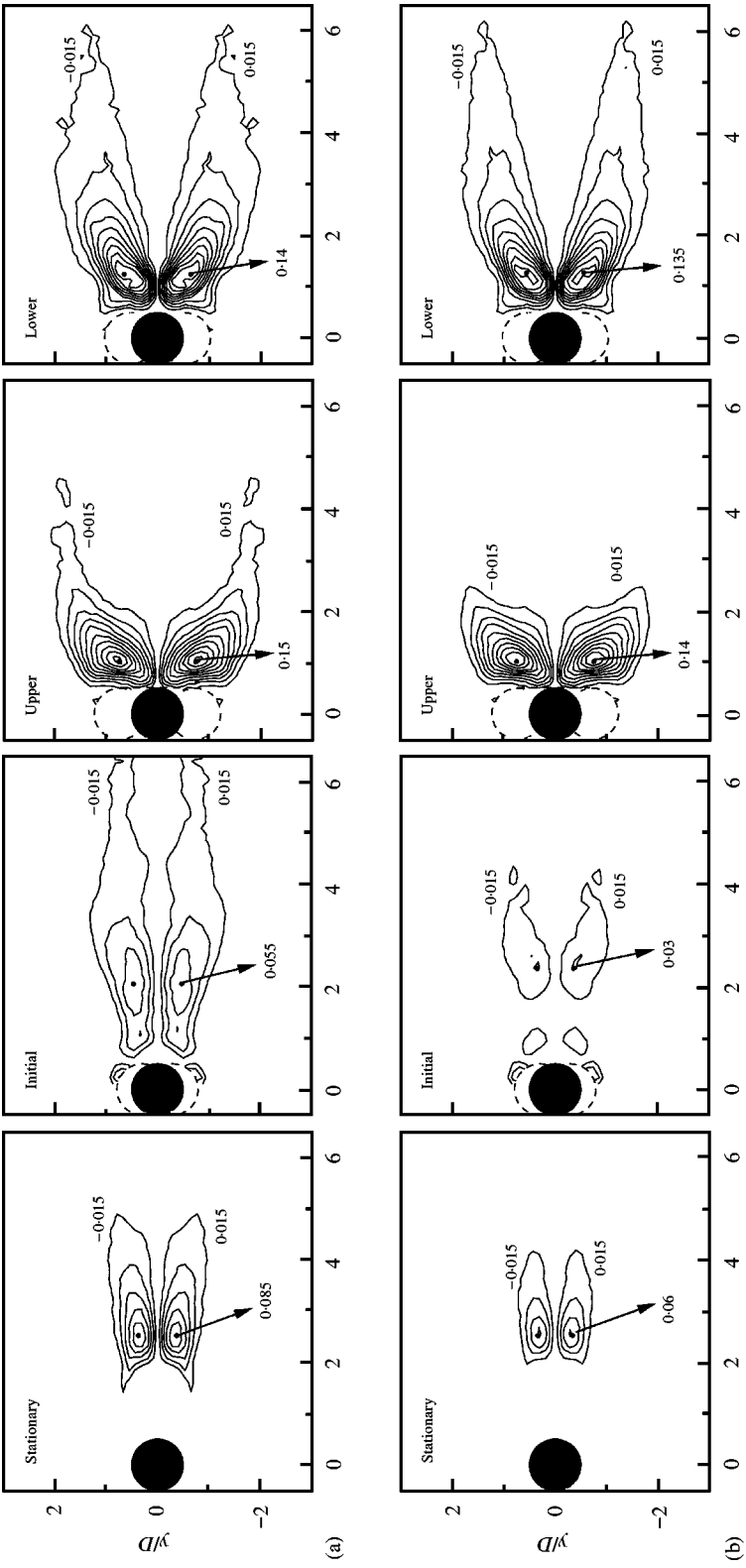

Figure 8. Contours of (a) total $(\overline{u''v''}/U^2)$ and (b) periodic component $(\overline{\tilde{u}\tilde{v}}/U^2)$ of the global mean Reynolds shearing stress. Contours shown are separated by 0·015 for all the cases. ●, location of the maximum value of the Reynolds stress.

TABLE 2
Peak periodic Reynolds stress ($\overline{\tilde{s}\tilde{s}}$) as a percentage of peak total Reynolds stress ($\overline{s''s''}$)

	Stationary (%)	Initial (%)	Upper (%)	Lower (%)
$(\overline{\tilde{u}\tilde{u}}/\overline{u''u''})$	59	89	96	95
$(\overline{\tilde{v}\tilde{v}}/\overline{v''v''})$	78	93	93	90
$(\overline{\tilde{u}\tilde{v}}/\overline{u''v''})$	71	55	93	96

TABLE 3
Vortex formation length (l_f)

	Stationary	Initial	Upper	Lower
$(l_f/D)_{\text{closure point}}$	2·27	1·46	—	—
$(l_f/D)_{\text{location of max } \overline{u''u''}}$	2·33	0·55	0·64	0·68

part is approximately 60% of the total Reynolds stress. In Table 2, we present percentages for the ratios of periodic to total stress, for the three different Reynolds stresses, and corresponding to each of the three cylinder response branches as well as for the stationary cylinder (see Figures 6–8). A striking feature of Table 2, is the increase in percentages for the oscillating cylinder cases, to about 90% or greater, in contrast to the approximately 70% level for the stationary cylinder. This would indicate that for the oscillating cylinder, nearly all the total Reynolds stress comes from the large-scale periodic dynamics of the flow. The above point, combined with the fact that these large-scale periodic coherent structures seem to be relatively independent of Re, as noted previously in comparison to Cantwell & Coles (1983), would indicate that the Reynolds stresses measured in the present work, for the oscillating cylinder at Re = 3000–4000, would be quite representative also of much higher Reynolds numbers; a point that could be useful in modelling these problems. [It may be noted in Table 2, that unlike all the other cases, the percentage of the periodic shearing stress ($\overline{\tilde{u}\tilde{v}}/U^2$) in the Initial branch, is quite small, about 55% of the total shearing stress. The reason for the low value in this particular case is not known at present.]

The numerical values of the peak periodic stress, and indeed the peak total stress, can be considerably larger for an oscillating cylinder, compared to the stationary cylinder, as may be seen from Figures 6–8. In particular, the largest increase in periodic stress appears to be for the Lower branch of cylinder response, which corresponds to the 2P-mode, where $(\overline{\tilde{u}\tilde{u}}/U^2)_{\max}$ increases by 485%, $(\overline{\tilde{v}\tilde{v}}/U^2)_{\max}$ increases by 100%, and $(\overline{\tilde{u}\tilde{v}}/U^2)_{\max}$ increases by 125%, compared to the stationary cylinder values, which seem to be relatively independent of Re. This large increase in the periodic Reynolds stresses in the Lower branch is consistent with the large increase (of about 200%) in the total circulation that is shed into the large-scale vortices, as discussed in Govardhan & Williamson (2000). The increased vortex circulation corresponds with the large increase in fluctuating lift (by a factor of 6), and in mean drag (by a factor of 5), as shown in Khalak & Williamson (1997).

We shall now briefly look at the "formation length" for the oscillating cylinder. Contour plots of the total streamwise Reynolds stress ($\overline{u''u''}$) in the wake, shown in Figure 6, indicate that the location of the maximum value of $\overline{u''u''}$ gets closer to the cylinder when it vibrates, compared to the stationary cylinder, consistent with the observations of Griffin (1971), and with our earlier observation of a reduction in the size of the recirculation bubble. The formation length (l_f) has been defined in many ways as discussed recently by Noca *et al.*

(1998) and by Norberg (1998). In Table 3, we show values of l_f calculated from the 'closure point' ($\bar{u}/U = 0$ on wake centreline), and from the streamwise location of maximum $\overline{u''u''}$ in the wake; in each case l_f is measured from the cylinder axis. It can be seen that l_f (computed in either of the two ways) is considerably reduced for the oscillating cylinder compared to the stationary cylinder. However, at the present Re = 3000–4000, the reduction in l_f is substantially greater than that observed by Griffin at Re $\approx$ 200. In fact, it is interesting to note that one cannot define l_f based on the closure point for the Upper and Lower branches, as there is no recirculation bubble in these cases. The formation length can however still be calculated based on the streamwise location of maximum $\overline{u''u''}$ in the wake, which gives values of $l_f/D \approx 0{\cdot}6$, which is substantially lower than the smallest values of $l_f/D \approx 1{\cdot}6$ reported by Griffin at Re $\approx$ 200.

5. CONCLUSIONS

In this work, we study the wake velocity field of an elastically mounted rigid cylinder that is constrained to move transverse to the free stream, using DPIV measurements.

The measured mean velocity fields indicate that the characteristic "recirculation bubble", usually seen in the mean velocity field behind the nonoscillating cylinder, is present in the case of the '2S' wake formation mode, but is completely absent for the 2P-mode. For the '2P' mode, we find instead the appearance of a pair of counterrotating vortices of opposite sign to what is expected, causing a downstream oriented jet-type flow close to the cylinder, which in turn results in a 'double-wake' type velocity profile.

We evaluate the total Reynolds stresses, and the periodic component of stress, computed from phase-averaged velocity data, for the stationary cylinder as well as for the oscillating cylinder in each of the three response branches, namely the Initial, Upper and Lower branches. Comparison of the stationary cylinder peak stresses, at Re = 3900, with the data of Cantwell & Coles (1983), at much higher Re (Re = 140 000), indicate that although the total Reynolds stresses are significantly larger at the higher Reynolds numbers, the periodic component of stress is quite similar in both cases. This suggests that the repeatable large-scale coherent structures, responsible for the periodic part of the Reynolds stresses, are quite similar over the wide range of Re from 3900 to 140 000. In the case of the oscillating cylinder, typically more than 90% of the total Reynolds stresses are due to these repeatable large-scale coherent structures. The above facts suggest that the Reynolds stresses obtained in the present work, at Re $\approx$ 3900 for the oscillating cylinder, would be quite representative also of much higher Re cases; a point that could be useful in modelling these problems.

Reynolds stresses at different constant phases of vortex shedding, corresponding to each of the three cylinder response modes, have also been computed, but are not included in this paper, for brevity.

ACKNOWLEDGEMENTS

The support from the Ocean Engineering Division of O.N.R., monitored by Dr. Tom Swean, is gratefully acknowledged (O.N.R. Contract Nos. N00014-94-1-1197 and N00014-95-1-0332).

REFERENCES

BEARMAN, P. W. 1984 Vortex shedding from oscillating bluff bodies. *Annual Review of Fluid Mechanics* **16,** 195–222.

BRIKA, D. & LANEVILLE, A. 1993 Vortex-induced vibrations of a long flexible circular cylinder. *Journal of Fluid Mechanics* **250,** 481–508.

CANTWELL, C. & COLES, D. 1983 An experimental study of entrainment and transport in the turbulent near wake of a circular cylinder. *Journal of Fluid Mechanics* **136,** 321–374.

CARBERRY, J., SHERIDAN, J. & ROCKWELL, D. 2001 Forces and wake modes of an oscillating cylinder. *Journal of Fluids and Structures* **15,** 523–532.

GOVARDHAN, R. & WILLIAMSON, C. H. K. 2000 Modes of vortex formation and frequency response of a freely-vibrating cylinder. *Journal of Fluid Mechanics* **420,** 85–130.

GRIFFIN, O. M. 1971 The unsteady wake of an oscillating cylinder at low Reynolds number. *Journal of Applied Mechanics* **38,** 729–738.

KHALAK, A. & WILLIAMSON, C. H. K. 1997 Fluid forces and dynamics of a hydroelastic structure with very low mass and damping. *Journal of Fluids and Structures* **11,** 973–982.

KHALAK, A. & WILLIAMSON, C. H. K. 1999 Motions, forces and mode transitions in vortex-induced vibrations at low mass-damping. *Journal of Fluids and Structures* **13,** 813–851.

KOOCHESFAHANI, M. M. 1989 Vortical patterns in the wake of an oscillating airfoil. *AIAA Journal* **27,** 1200–1205.

NOCA, F., PARK, H. G. & GHARIB, M. 1998 Vortex formation length of a circular cylinder ($300 < \mathrm{Re} < 4000$) using DPIV. In *Proceedings of the 1998 Conference on Bluff Body Wakes and Vortex-Induced Vibration, Washington DC* (eds P. W. Bearman & C. H. K. Williamson), Paper No. 46, Ithaca, NY: Cornell University.

NORBERG, C., 1998 LDV-measurements in the near wake of a circular cylinder. In *Proceedings of the 1998 Conference on Bluff Body Wakes and Vortex-Induced Vibration* (eds P. W. Bearman & C. H. K. Williamson), Paper No. 42, Ithaca, NY: Cornell University.

PARKINSON, G. 1989 Phenomena and modelling of flow-induced vibrations of bluff bodies. *Progress in Aerospace Sciences* **26,** 169–224.

ROSHKO, A. 1993 Perspectives on bluff body aerodynamics. *Journal of Wind Engineering and Industrial Aerodynamics* **49,** 79.

REYNOLDS, W. C. & HUSSAIN, A. K. M. F. 1972 The mechanics of an organized wave in turbulent shear flow. Part 3. Theoretical models and comparisons with experiments. *Journal of Fluid Mechanics* **54,** 263–288.

SARPKAYA, T. 1979 Vortex-induced oscillations. *Journal of Applied Mechanics* **46**, 241–258.

SCHILLER, L. & LINKE, W. 1933 Pressure and frictional resistance of a cylinder at Reynolds numbers 5000 to 40,000. NACA TM 715.

STANSBY, P. K. & APSLEY, D. D. 2000 Flow around cylinders: modelling, dynamic response, arrays. In *Proceedings of the Workshop on Vortex-Induced Vibrations of Offshore Structures* (eds C. P. Pesce, C. A. Martins, J. R. Meneghini & J. A. P. Aranha), pp. 32-34, São Paulo, Brazil: Universidade de São Paulo.

TECHET, A. H., HOVER, F. S., & TRIANTAFYLLOU, M. S. 1998 Vortical patterns behind a tapered cylinder oscillating es transversely to a uniform flow. *Journal of Fluid Mechanics* **363,** 79–96.

WILLIAMSON, C. H. K. 1996 Vortex dynamics in the cylinder wake. *Annual Review of Fluid Mechanics* **28,** 477–539.

WILLIAMSON, C. H. K. & ROSHKO, A. 1988 Vortex formation in the wake of an oscillating cylinder. *Journal of Fluids and Structures* **2,** 355–381.